ORIGIN OF *EXO* SELECTIVITY IN NORBORNENE. AN *AB INITIO* MO STUDY

NOBUAKI KOGA, TADAHIRO OZAWA* AND KEIJI MOROKUMA†

Institute for Molecular Science, Myodaiji, Okazaki 444, Japan and Tochigi Research Laboratories, Kao Corporation, Ichikai 321-34, Japan

The geometries of the reactants, the reactant π-complex, the transition state and the product for *exo* and *endo* addition of BH_3 to norbornene were optimized at the HF/3–21G level, and their energies were calculated at the MP2/6–31G level. The analysis of activation energy and model calculations singled out the *endo* deformability, a major portion of the norbornene deformation energy, as the origin of *exo* selectivity; norbornene, with the olefinic hydrogens already bent toward *endo* in the equilibrium geometry, requires less deformation to reach the *exo* than the *endo* transition state. The reason why olefinic hydrogens are bent in norbornene has been elucidated. An analysis indicates that the difference between norbornene *exo* side and bicyclo[2.2.1]hex-2-ene is also dictated by the *endo* deformability.

INTRODUCTION

A very high *exo* selectivity (*exo/endo* = 200:1) was found by Brown[1] in the hydroboration of norbornene (1) (equation 1).

$$(1)$$
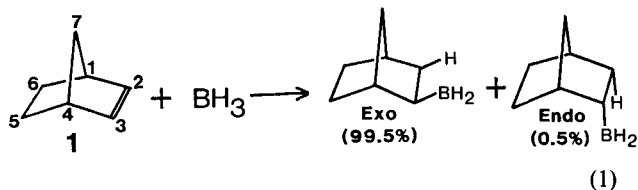
Norbornene *exo* side has been found to be more reactive than ethylene, which in turn is more reactive than norbornene *endo* side.[2] The stereoselectivity has been studied for various norbornene derivatives in many reactions, including hydroboration,[1,3] epoxidation[4,5] and Diels–Alder reactions.[5–7] Many proposals have been made concerning the origins of the *exo* selectivity of norbornene and related compounds.

The torsional effect was proposed by Schleyer[8] for the *exo* selectivity in the deuteration of norbornan-2-one enolate ion (2). The dihedral angle between C-3 and C-4 substituents around the C-3—C-4 axis is about 20° in the reactant (2). In the transition state for the *exo* attack (3) this angle is increased, to release the torsional strain. On the other hand, for the *endo* attack (4), the angle is reduced, to increase the strain energy in the
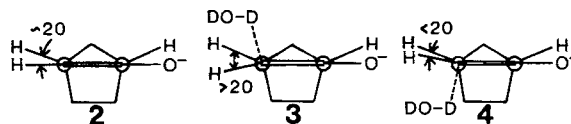
transition state. Hence the *exo* attack takes place more easily than the *endo* attack.

The steric effect, proposed by Brown,[1] is based on experimental results in hydroboration that norbornene gave a 99·5% *exo* product, whereas 7,7-dimethylnorbornene (5) showed an *endo* selectivity with a 78:22 ratio [equation (2)].
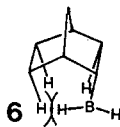
$$(2)$$
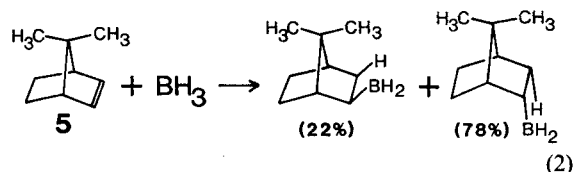
In norbornene, the steric hindrance[1a] (6) of the BH_3 with the ethano bridge hydrogens makes *endo* attack less favourable. On the other hand, in 5 bulky CH_3 groups on the methano bridge makes the *exo* attack sterically undesirable.

The non-equivalent orbital extension, proposed by Inagaki *et al.*,[9] suggests that the higher *exo* reactivity


6

in norbornene is due to the higher HOMO electron density on the *exo* side than on the *endo* side caused by mixing of σ orbitals and π orbitals.

The staggering effect, proposed by Rondan *et al.*,[10] gives consideration to the new bonds being formed. In the cycloaddition of fulminic acid to norbornene, the transition state calculated with an *ab initio* MO method suggests that the newly formed C—O and C—C bonds have a larger overlap (smaller θ) with the ethano bridge in the *endo* transtion state (**7**) than with the methano bridge in the *exo* transition state (**8**). The *exo* attack with less overlap and less repulsion is preferred.


7   **8**
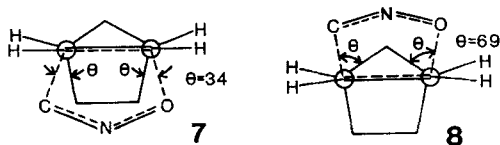
The *endo* deformability effect, first proposed by Wipff and Morokuma[11] and later elaborated by Spanget-Larsen and Gleiter,[12a,b] considers that the *exo* side is more reactive than the *endo* side because the olefin part of isolated norbornene is already non-planar with its hydrogen atoms bent to the *endo* side. Further bending to reach the transition state for the *exo* reaction requires less energy than for the *endo* reaction, where bending all the way back to the *exo* side is required. Calculations with a semiempirical MO method indicated that bending of the olefinic hydrogen atoms from a coplanar geometry to the *endo* side, say by 20°, requires over 0·1 eV less energy than that to the *exo* side.[12a,b] Calculations at the HF/STO-3G level also support this proposal.[12c]

Some of these theories base their argument on the properties of isolated reactants, some on the interaction of rigid reactants and some on transition states. Some theories seem to share a common concept of steric repulsion. Every theory, however, without knowing exactly what the transition states are like, arbitrarily picks a 'favourite' factor and proposes its importance intuitively, and seems to lack decisive evidence substantiating the claims. What is needed is an evaluation of contributions of various factors to the transition-state energy difference between the *exo* and *endo* attack.

In this paper, after a brief description of the method, an *ab initio* calculation is used to determine both the *exo* and the *endo* transition states for hydroboration of norbornene, analysing the difference in the barrier heights in terms of the deformation and the interaction energy. Further, models are built and energetic contri-

butions of the various proposals mentioned above are evaluated. After the predominant origin of the *exo* selectivity has been identified to be the *endo* deformability, an attempt is made to establish why the olefin hydrogens in isolated norbornene are bent. Finally, bicyclo[2.2.1]hex-2-ene (**9**) and norbornene are compared.

9
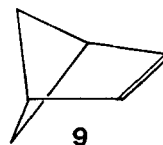
METHODS OF CALCULATION

The geometries of the reactants and transition states were fully optimized at the HF/3-21G[13] level, unless stated otherwise. The energetics were calculated also with the Møller–Plesset second-order perturbation theory (MP2)[14] with the 6-31G[15] basis set at the HF/3-21G optimized geometries. The GAUSSIAN82 program[16] was used.

EXO AND *ENDO* ADDITION OF BH₃ TO NORBORNENE

Geometries and energetics for *exo* and *endo* addition to norbornene

The HF/3-21G optimized geometry of norbornene, shown in Figure 1, has the olefin carbon atoms pyramidal, with the hydrogen atoms bent toward the *endo* side. We define the pyramidalization or bending angle as 180° minus the dihedral angle between HC-2 and C-2—C-1 (and also between HC-3 and C-3—C-4) with respect to the C-2—C-3 axis with the positive (negative) sign for *endo* (*exo*) bending. The bending angle calculated with various *ab initio* methods[11,12,17] and the empirical molecular mechanics (MM2)[17b] are summarized in Table 1. In all cases the bending is to the *endo* side, from a few to several degrees.
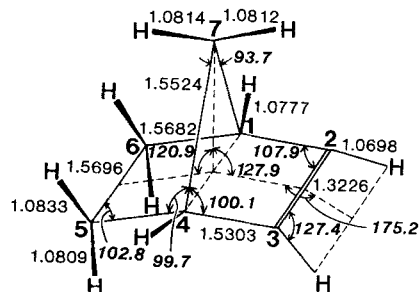

Figure 1. HF/3-21G optimized geometry of norbornene. In this and other structures bond lengths are in Å and angles in degrees

Table I. Bending angle of norbornene at various levels of calculation

Method	Angle ($^\circ$)			
MM2	$1\cdot7^a$			
HF/STO–3G	$4\cdot9,^b$	$3\cdot4,^c$	$4\cdot3,^a$	$3\cdot9^d$
HF/3–21G	$4\cdot8^e$			

[a] Ref. 17b.
[b] Ref. 10.
[c] Ref. 17a.
[d] Ref. 12c.
[e] This work.

The optimized geometries of the *exo* and *endo* transition states and the corresponding reactant complexes and products for addition of BH_3 are shown in Figure 2. In the optimization, the CH bond distances that are away from the reactive centres (C-1—H, C-4—H, C-5—H, C-6—H and two C-7—Hs, as shown in bold lines in Figure 1) are assumed to be those of norbornene itself in Figure 1.

The potential energy profiles at the HF/3-21G and MP2/6–31G levels are shown in Figure 3, together with that for ethylene + BH_3. [There is some doubt whether any activation energy exists for the reaction of BH_3 with norbornene in the gas phase. For instance, the MP2/6–31G* optimization for the reaction of BH_3 with the less reactive ethylene shows that the potential surface is downhill from the reactants, without π-complex or transition state, to the 1,2-addition product.[19a] The only corresponding experimental result shows a marginal positive activation energy of 2 ± 3 kcal mol^{-1}.[19b] Despite the above results, the present use of E_a or E_b for comparison of reactivity in solution is justifiable as follows. On the reactant side BH_3 is stabilized by forming a complex with solvent tetrahydrofuran molecules.[1] At the transition state BH_3 interacts strongly with norbornene and little, if any, solvation is expected to take place. The real barrier, therefore, is the sum of the

Figure 2. HF/3–21G optimized geometries of *exo* and *endo* reactant complexes, transition states and products of BH_3 addition to norbornene. Corresponding ethylene results are shown for comparison. Only essential geometrical parameters are shown. The CH bond distances that are shown in bold lines in Fig. 1 are fixed (see text)

desolvation energy of BH_3 and the intrinsic barrier E_a. Since the desolvation energy is independent of the substrate, the *exo – endo* difference is determined by the intrinsic barrier. In this paper, we also use different levels of calculation to show that, although the calculation is far from 'converged' with respect to the basis set and the electron correlation, the present analysis leads to the same conclusion as to the origin of *exo* selectivity

at all the levels of calculation.] The energies of the transition state relative to the reactants and the reactant complex are calculated as E_a and E_b and are shown in Tables 2 and 3, respectively. Regardless of consideration of E_a or E_b, and regardless of the level of calculation, the *exo* barrier of norbornene is lower than that of ethylene, which in turn is lower than the *endo* barrier of norbornene, in agreement with experiment.[2]
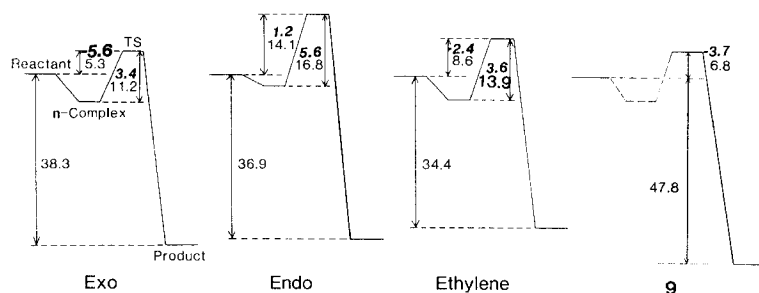
Figure 3. Potential energy profiles (in kcal mol^{-1}) for norbornene, ethylene and 9 + BH_3 at the HF/3–21G, and the MP2/6–31G level (in italics) at the HF/3–21G optimized geometries

Table 2. Deformation (*DEF*) and interaction (*INT*) energy contributions to *exo* and *endo* barriers (E_a = transition state – reactants)[a]

Method	Component	Exo	Ethylene	Endo	Δ(exo – endo)	Δ(exo – ethylene)
HF/3–21G	E_a	5·3	8·6	14·1	−8·8	−3·3
	DEF(norb)[b]	14·2	12·5	20·8	−6·6	1·7
	DEF(BH₃)	22·6	23·2	21·8	0·8	−0·6
	INT	−31·5	−27·1	−28·6	−2·9	−4·4
MP2/6–31G	E_a	−5·6	−2·4	1·2	−6·8	−3·2
	DEF(norb)[b]	7·2	6·9	13·1	−5·9	0·3
	DEF(BH₃)	21·5	22·1	20·8	0·7	−0·6
	INT	−34·3	−31·4	−32·7	−1·6	−2·9

[a] Energies in kcal mol^{-1} at the HF/3–21G optimized geometries. The total energies in the *exo* transition state are −295·5979 (HF/3–21G) and −297·8153 hartree (MP2/6–31G).
[b] For ethylene, this is *DEF*(C_2H_4).

Table 3. Deformation (*DEF*) and interaction (*INT*) energy contributions to *exo* and *endo* barriers (E_b = transition state – reactant complex)[a]

Method	Component	Exo	Ethylene	Endo	Δ(exo – endo)	Δ(exo – ethylene)
HF/3–21G	E_b	11·2	13·9	16·8	−5·6	−2·7
	DEF(norb)[b]	13·8	12·4	20·6	−6·8	1·4
	DEF(BH₃)	20·4	22·0	21·6	−1·2	−1·6
	INT	−23·0	−20·5	−25·4	2·4	−2·5
MP2/6–31G	E_b	3·4	3·6	5·6	−2·2	−0·2
	DEF(norb)[b]	7·5	7·3	13·3	−5·8	0·2
	DEF(BH₃)	19·5	20·9	20·6	−1·1	−1·4
	INT	−23·6	−24·6	−28·3	4·7	1·0

[a] Energies in kcal mol^{-1} at the HF/3–21G optimized geometries.
[b] For ethylene, this is *DEF*(C_2H_4).

With this agreement in mind, we analyse the differences in the activation energies between the *exo* and *endo* reactions of norbornene, $\Delta E_a = E_a(exo) - E_a(endo)$ and $\Delta E_b = E_b(exo) - E_b(endo)$, and determine the origin of *exo* selectivity. (See the discussion in brackets above.)

Deformation and interaction contribution to the *exo – endo* barrier difference

The activation energy differences between *exo* and *endo* reactions, ΔE_a and ΔE_b, were analysed in terms of deformation and interaction contributions.[20] In this analysis, both reactants are first deformed to the geometries which they take at the transition state, which requires the deformation energy *DEF*, and then the deformed reactants are allowed to interact with each other gaining the interaction energy *INT*:

$$\Delta E_a = E_a(exo) - E_a(endo)$$
$$= \Delta DEF(\text{norb}) + \Delta DEF(\text{BH}_3) + \Delta INT$$

A similar decomposition can be done for ΔE_b, where the energy components of the reactant complex are subtracted from those of the transition state.

Tables 2 and 3 show the ΔDEF and ΔINT contributions to ΔE_a and ΔE_b, respectively, at two levels of calculation at the HF/3–21G optimized geometries. At all levels, the deformation energy contribution of the norbornene part, $\Delta DEF(\text{norb})$, is predominant. Its magnitude changes little between E_a and E_b or among HF/3–21G and MP2/6–31G. This leads to the most

important conclusion about the origin of the *exo* selectivity, that the energy required to deform norbornene to reach the transition state, from either the reactant or the reactant complex, is smaller in the *exo* than in the *endo* reaction. Table 2 shows that the interaction energy difference ΔINT also makes a small but nonnegligible contribution to ΔE_a, although its weight is reduced by the introduction of the MP2 correlation effect. One can see in Table 3, however, that the ΔINT contribution to ΔE_b is positive, indicating that the difference in *INT* is more important in the π-complex than in the transition state.

Detailed comparison of the transition state geometries

In order to elucidate further the *exo–endo* difference and its origin, we compared in detail the HF/3–21G optimized geometries of the *exo* and the *endo* transition states, shown in Figure 2. A comparison of the four-atom reaction centres, shown in Figure 4, indicates that in the *endo* transition state the C-2⋯B and the C-3⋯H distances are longer by about $0 \cdot 02$–$0 \cdot 03$ Å and the C-2—C-3 and the H—B distances are shorter by about $0 \cdot 006$–$0 \cdot 01$ Å than in the *exo* transition state, suggesting that the former is at an earlier stage of reaction than the latter. As shown in Figure 3, the difference in exothermicity of the reaction is substantially smaller than that in the transition state. Therefore, this earliness of the *endo* transition state is not caused by the difference in exothermicity, but rather is considered
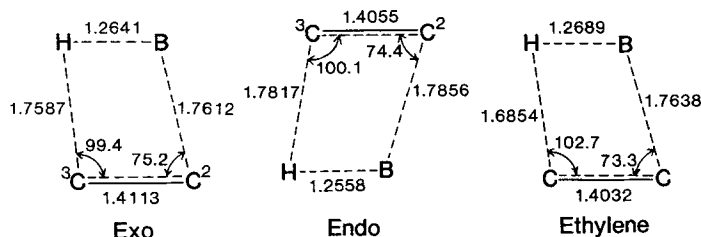

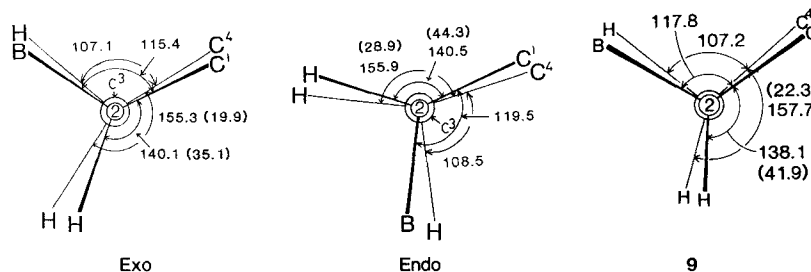Figure 4. Geometries of four-atom reaction centres

Figure 5. Dihedral angles around the C-2—C-3 axis at the transition states. Numbers in parentheses are changes from the reactant

to come from the difficulty of approach between the reactants.

A detailed comparison of the dihedral angles of substituents around the C-2—C-3 axis is shown in Figure 5. The direction of approach of attacking H and B with respect to the norbornene carbon skeleton is 115° and 107°, respectively, in the *exo* transition state, compared with 120° and 109°, respectively, in the *endo* transition state, indicating that the attack takes place from further outside in the *endo* than in the *exo* reaction.

Figure 6 shows the dihedral angles between the norbornene skeleton carbon atoms and the methano C-7 atom with respect to the C-1—C-4 axis. Those of C-5 and C-6, far away from the reactive centre, have not changed much (<1·6°) from the norbornene values. The changes in the C-2 and C-3 dihedral angles are larger; the *exo* attack increases the angles by 1·4° and 2·8°, respectively, pushing these carbon atoms down to the *endo* side, whereas the *endo* attack decreases the angles, by 4·1° and 6·5°, pushing C-2 and C-3 up to the *exo* side. These trends in changes of the dihedral angles, seen in Figures 5 and 6, clearly indicate that repulsion occurs between norbornene and the attacking reagent, the *endo* attack having larger angle changes and hence a larger steric repulsion. These characteristics are more clearly observed in the π-complexes (Figure 2), where the interaction is weaker. Whereas the shortest H····H distance between BH_3 and norbornene is about 2·56 Å in both the *exo* and *endo* complexes, the shorter B····C distance is about 2·51 Å in the *exo* and 3·02 Å in the *endo* complex. Obviously, the existence of steric

repulsion in the *endo* complex prevents the approach and thus reduces the attractive interaction between BH_3 and norbornene.

These geometrical considerations suggest that some steric repulsion might be an important factor determining the *exo* selectivity of norbornene. These structural analyses, however, do not indicate what the energetic contribution is.

Models in the search for the origins of *exo* selectivity

In order to assess the energetic contributions of various effects to ΔE_a, we shall construct several models that represent these effect as even-handedly as possible, and compare them. The main reasons why we choose ΔE_a instead of ΔE_b are that all the existing theories of *exo* selectivity consider, implicity or explicitly, changes from the reactants and that ΔE_a is easier to interpret than ΔE_b. Recognizing that ΔE_b may be a better measure for solution reactions, we shall later examine contributing factors to ΔE_b.

Staggering effect [10]

The dihedral angles between bonds around the C-2—C-1 and the C-3—C-4 axes are shown in Figure 7 for the transition states. In the *exo* transition state, the newly formed bonds C-2····B and C-3····H roughly bisect the C-7—C-1—H and the C-7—C-4—H angles, respectively, and are essentially staggered, whereas in the *endo* transition state, the C-2····B bond is nearly eclipsed with the C-1—C-6 bond with a dihedral angle of 9·1°. As
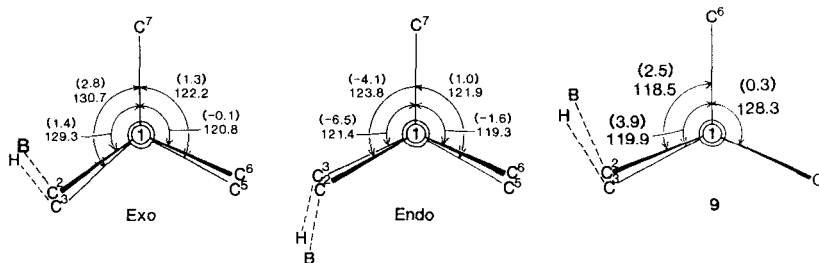

Figure 6. Dihedral angles around the C-1—C-4 axis at the transition states. Numbers in parentheses are changes from the reactant
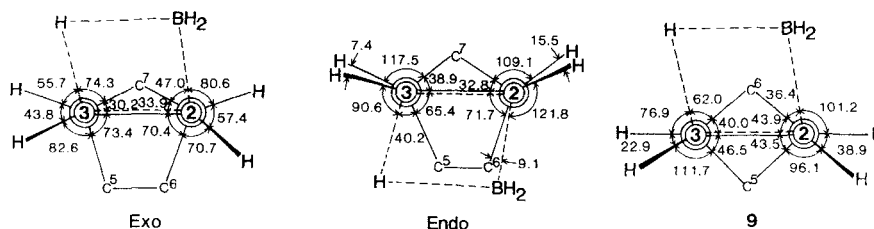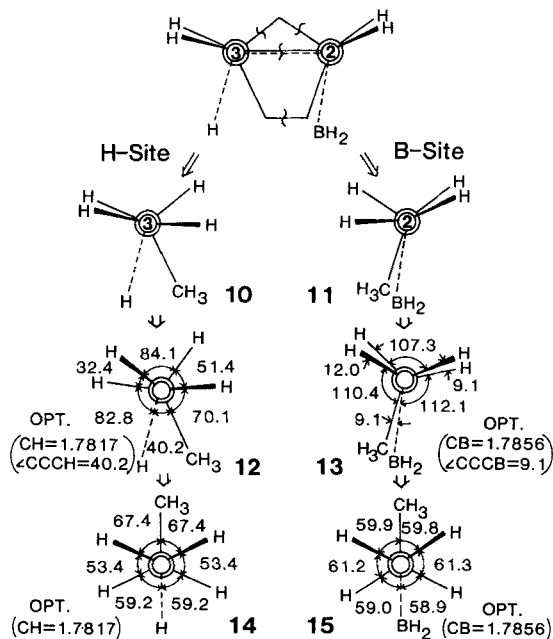

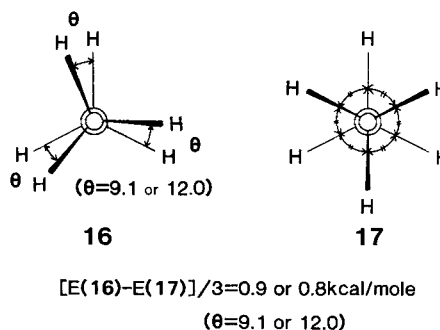Figure 7. Dihedral angles around the C-2—C-1 and the C-3—C-4 axis at the transition states

Scheme 1. Model for staggering effect (*endo*)

$[E(16)-E(17)]/3=0.9$ or $0.8kcal/mole$

$(\theta=9.1$ or $12.0)$

Scheme 2. Model for staggering effect (CH—CH repulsion)

suggested by Rondan *et al.*,[10] this would make the *endo* transition state less favourable.

In order to estimate the energetic contribution of the C-2····B and C-1—C-6 bond overlap and the C-3····H and C-4—C-5 bond overlap, we construct the following model. As shown in Scheme 1 for the *endo* transition state, we cut four C—C bonds and divide the system into two fragments (10 and 11), where the broken C—C bonds are replaced by C—H bonds having a standard bond length of $1 \cdot 0777$ Å. The geometry of fragment 11 is at first fully optimized, except that the C-2····B distance and the B—C-2—C-1—CH₃ dihedral angle are fixed at the transition state values of $1 \cdot 7856$ Å and $9 \cdot 1°$, respectively. In the resulting structure 13, all the strain energy existing in the transition state has been released except for that associated with the C-2····B bond length and the overlap of bonds across the C-2—C-1 bond. Next the geometry is fully reoptimized except for the fixed C-2····B distance. In the resulting structure 15, the strain energy associated with the bond overlap is also released. The energy difference, $E(13) - E(15)$, calculated to be $4 \cdot 0 \, \text{kcal mol}^{-1}$ (HF/3-21G), is the destabilization energy due to the bond overlap across the C-2—C-1 bond. However, this energy difference contains, in addition to the targeted overlap repulsion between C-2····B and C-1—C-6, the repulsion between the nearly eclipsed CH bonds, since

the HCCH dihedral angles are very small ($9 \cdot 1°$ and $12 \cdot 0°$) in 13.

An estimate of the CH—CH repulsions has been made in Scheme 2. The structure of ethane is optimized (16) under C_{3v} symmetry with the additional constraint of (all three) HCCH dihedral angles θ of $9 \cdot 1°$ or $12 \cdot 0°$. The energy difference between the energy of 16 and that of the fully optimized ethane (17, with D_{3d} symmetry) is three times the overlap repulsion between nearly eclipsed CH bonds. The calculated value of the CH—CH repulsion energy is $0 \cdot 9$ and $0 \cdot 8 \, \text{kcal mol}^{-1}$ for $\theta = 9 \cdot 1°$ and $12 \cdot 0°$, respectively. Subtracting the CH—CH repulsion energies from the total overlap repulsion energy, $E(13) - E(15)$, one obtains the repulsion energy between C-2····B and C-1—C-6 as $4 \cdot 0 - 0 \cdot 9 - 0 \cdot 8 = 2 \cdot 3 \, \text{kcal mol}^{-1}$.

Similar calculations were also carried out for the fragment 10 in Scheme 1 with the sequence of 12 and 14. The energy difference $E(12) - E(14) = 0 \cdot 4 \, \text{kcal mol}^{-1}$ is found (by the method in Scheme 2) to be dominated by the CH—CH repulsion ($32 \cdot 4°$ and $51 \cdot 4°$), and therefore the repulsion energy between C-3····H and C-4—C-5 is estimated to be $0 \cdot 0$. Therefore, the total overlap repulsion between the newly formed C-2····B and C-3····H bonds and norbornene at the *endo* transition state is $2 \cdot 3 + 0 \cdot 0 = 2 \cdot 3 \, \text{kcal mol}^{-1}$.

A corresponding calculation was carried out also for the *exo* transition state, based on Scheme 3. The total overlap repulsion between the new C-2····B and C-3····H bonds and norbornene at the exo transition state is $0 \cdot 3 + 0 \cdot 0 = 0 \cdot 3 \, \text{kcal mol}^{-1}$. Taking the difference between *exo* and *endo* transition states, the contribution of the staggering effect is estimated to be $exo - endo = 0 \cdot 3 - 2 \cdot 3 = -2 \cdot 0 \, \text{kcal mol}^{-1}$.
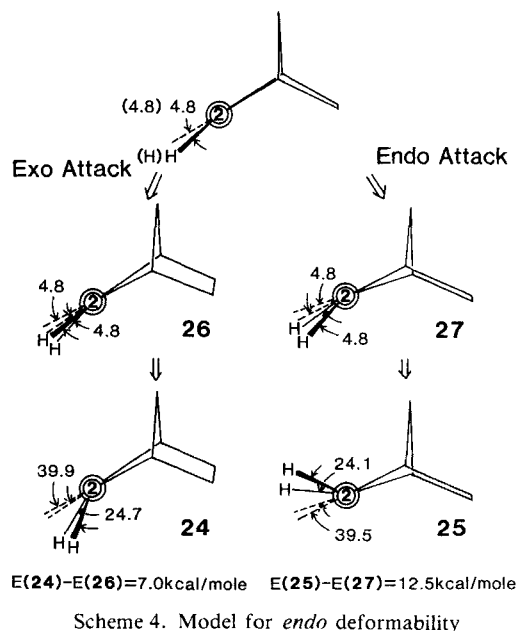
The staggering effect reflects the stability of the newly formed bonds and is part of the interaction energy term ΔINT. The staggering effect $(-2 \cdot 0 \, \text{kcal mol}^{-1})$ accounts for about two thirds of the total interaction energy difference ΔINT $(-2 \cdot 9 \, \text{kcal mol}^{-1})$.
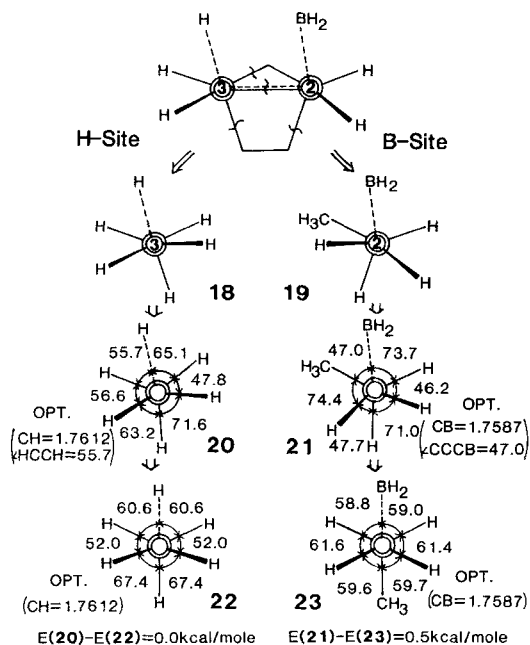
Scheme 3. Model for staggering effect (*exo*)

Scheme 4. Model for *endo* deformability

ENDO *deformability*[11,12] *and torsional effect*[8]

As shown in Figure 5, the dihedral angles of olefinic hydrogens with respect to the C-2—C-3 axis measured from the C-1—C-2 and the C-4—C-3 bonds are 140·1° and 155·3°, respectively, for the *exo* transition state and 140·5° and 155·9°, respectively, for the *endo* transition state. The bending angles in the *exo* transition state are essentially the same as those in the *endo* transition state. In norbornene itself, as shown in Figure 1, they are 175·2°, i.e., the olefin hydrogens are bent down toward the *endo* side by 4·8° at the present level of calculation. The changes in these bending angles from the reactant to the *exo* transition state, 175·2 − 140·1 = 35·1° and 175·2 − 155·3 = 19·9°, are smaller than those for the *endo* transition state, 360 − 175·2 − 140·5 = 44·3° and 360 − 175·2 − 155·9 = 28·9°. The *endo* transition state requires a bending motion larger than the *exo* transition state by about 9°. This larger bending would be energetically less favourable, as has been pointed out by Spanget-Larsen and Gleiter.[12a,b]

In order to assess the energy difference due to this difference in bending, we used the method shown in Scheme 4. The deformation of norbornene (1) from its equilibrium geometry to its geometry at the transition state (24 for *exo* and 25 for *endo*) is assumed to take place through an intermediate (26 for *exo* and 27 for *endo*). In the intermediate all the geometrical parameters are those of the transition state except for

the olefin hydrogen bending angles, which are assumed to be 4·8°, those of norbornene equilibrium geometry. The energy change in the first step, norbornene (1) to the intermediate (26 and 27), is the deformation energy due to change in the ring structure, and is calculated at the HF/3-21G level to be 7·2 kcal mol⁻¹ for the *exo* and 8·3 kcal mol⁻¹ for the *endo* transition state. The *exo* − *endo* difference, 7·2 − 8·3 = −1·1 kcal mol⁻¹, is the ring deformation contribution to the barrier height difference. The energy change in the second step, from the intermediate (26 and 27) to the transition state geometry (24 and 25), is the deformation energy due to changes in bending angles, and is calculated to be 7·0 kcal mol⁻¹ for the *exo* and 12·5 kcal mol⁻¹ for the endo transmission state. The *exo* − *endo* difference, 7·0 − 12·5 = −5·5 kcal mol⁻¹, is considered to be the *endo* deformability contribution.

We also estimated what portion of the *endo* deformability of −5·5 kcal mol⁻¹ could be attributed to the torsional effect according to Schleyer.[8] As can be seen in Figure 7, the dihedral angles between the olefin hydrogen atoms and the bridgehead hydrogen atoms in the *endo* transition state, 7·4° and 15·5°, are much smaller than those in the *exo* transition state, 43·8° and 57·4°, clearly disfavouring the *endo* transition state. The torsional effect can be estimated by evaluating these CH—CH overlap repulsions. Adopting the same method (Scheme 2) as we used in calculating CH—CH repulsion in the staggering effect, we calculated the energy of the fully optimized ethane (17) and that of the ethane optimized with a fixed value (7·4° or 15·5°) for the three HCCH dihedral angles θ (16). A

third of $E(16) - E(17)$, $0 \cdot 9 \, \text{kcal mol}^{-1}$ for $7 \cdot 4°$ and $0 \cdot 8 \, \text{kcal mol}^{-1}$ for $15 \cdot 5°$, is the estimate of torsional energy for the *endo* transition state. For the *exo* transition state, both HCCH angles are $43 \cdot 8°$ and $57 \cdot 4°$, and the torsional energy for these angles are estimated from the method in Scheme 2 to be $0 \cdot 1$ and $0 \, \text{kcal mol}^{-1}$, respectively. Hence, the torsional effect to the *exo* − *endo* barrier difference is $(0 \cdot 1 + 0 \cdot 0) - (0 \cdot 9 + 0 \cdot 8) = -1 \cdot 6 \, \text{kcal mol}^{-1}$.

Therefore, we conclude that, of the norbornene deformation energy contribution to the *exo* − *endo* barrier difference, $\Delta DEF(\text{norb} = -6 \cdot 6 \, \text{kcal mol}^{-1}$, the ring structure deformation accounts for $-1 \cdot 1 \, \text{kcal mol}^{-1}$ and the *endo* deformability of olefin hydrogens is responsible for $-5 \cdot 5 \, \text{kcal mol}^{-1}$, which includes a torsional effect of $-1 \cdot 6 \, \text{kcal mol}^{-1}$.

Steric effect[1]

As was discussed in the Introduction, the steric effect is reflected in the difference in the strain of the norbornene carbon skeleton in addition to the difference in the intermolecular distances between the *exo* and *endo* transition states. The strain energy difference of the carbon skeleton was estimated in the previous sub-section to be $-1 \cdot 1 \, \text{kcal mol}^{-1}$. The difference in the intermolecular difference may be considered to be responsible for the portion of the interaction energy difference ΔINT $(-2 \cdot 9 \, \text{kcal mol}^{-1})$ that is not attributable to the staggering effect $(-2 \cdot 0 \, \text{kcal mol}^{-1})$, and is therefore estimated to be $-0 \cdot 9 \, \text{kcal mol}^{-1}$. Furthermore, the steric effect is probably also responsible for the difference in the deformation energy of BH_3, $\Delta DEF(BH_3) = +0 \cdot 8 \, \text{kcal mol}^{-1}$. Adding all these, an estimate for the steric effect on ΔE_a is $(-1 \cdot 1) + (-0 \cdot 9) + (+0 \cdot 8) = -1 \cdot 2 \, \text{kcal mol}^{-1}$, slightly favouring the *exo* transition state. Although the definition of the steric effect is somewhat arbitrary concerning what should be included, the above method of

estimation is probably more or less consistent with the original definition.[1]

Origin of exo selectivity

Contributions of various 'origins' to the energy difference between the *exo* and *endo* transition states obtained above are summarized in Table 4. The *endo* deformability[11,12] contribution is the largest, followed by staggering effect[10] and steric effect.[1] The electron correlation does not change the conclusion, as is also shown in Table 4.

Therefore, we conclude that the origin of the *exo* selectivity is the *endo* deformability.

Endo *deformability contribution to* ΔE_b

Here we shall examine the contribution of the *endo* deformability to ΔE_b, the *exo* − *endo* difference in the activation barrier relative to the reactant π-complex. We can use the method in Scheme 4, except that instead of $175 \cdot 2°$ as the dihedral angles of the intermediates **26** and **27**, we have to use those of the reactant π-complexes (Figure 8). Results at the HF/3–21G level are:

exo: $E(24) - E(26) = 6 \cdot 9 \, \text{kcal mol}^{-1}$;
endo: $E(25) - E(27) = 12 \cdot 4 \, \text{kcal mol}^{-1}$;
endo deformability contribution $= 6 \cdot 9 - 12 \cdot 4$
$$= -5 \cdot 5 \, \text{kcal mol}^{-1};$$

and at the MP2/6–31G level:

exo: $E(24) - E(26) = 4 \cdot 9 \, \text{kcal mol}^{-1}$;
endo: $E(25) - E(27) = 10 \cdot 3 \, \text{kcal mol}^{-1}$;
endo deformability contribution $= 4 \cdot 9 - 10 \cdot 3$
$$= -5 \cdot 4 \, \text{kcal mol}^{-1}.$$

Here again the *endo* deformability is found to be the origin of the *exo* selectivity.

Table 4. Estimates of contributions of various factors to exo − endo transition state energy difference[a]

			Endo deformability	$-5 \cdot 5$
				$(-5 \cdot 8)$
			(includes torsional effect	$-1 \cdot 6)$
$\Delta DEF(\text{norb})$	$-6 \cdot 6$			
	$(-5 \cdot 9)$			
		$-1 \cdot 1$	Ring deformation	
$\Delta DEF(BH_3)$	$+0 \cdot 8$	$+0 \cdot 8$		
	$(+0 \cdot 7)$		Steric effect	$-1 \cdot 2$
		$-0 \cdot 9$		
ΔINT	$-2 \cdot 9$			
	$(-1 \cdot 6)$			
			Staggering effect	$-2 \cdot 0$
ΔE_a	$-8 \cdot 7$			$-8 \cdot 7$
	$(-6 \cdot 8)$			

[a] $E(exo) - E(endo)$ in kcal mol^{-1} at the HF/3–21G level. Numbers in parentheses are energies at the MP2/6–31G level.
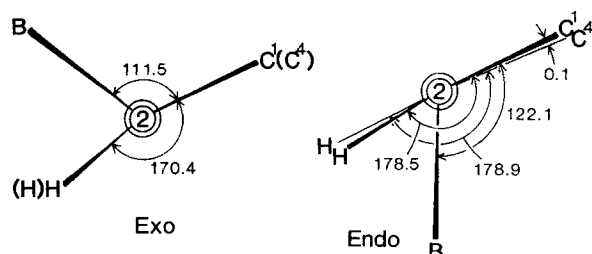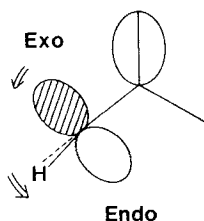
Figure 8. Dihedral angles around C-2—C-3 at the π-complexes

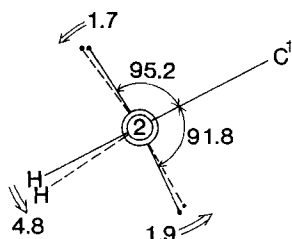## ORIGINS OF PYRAMIDALIZATION OF NORBORNENE

Structural considerations

It was found in the previous section that the principal origin of the *exo* selectivity of norbornene is the pyramidalization of olefinic hydrogens. The next question then is why the olefinic hydrogens are bent to the *endo* side.
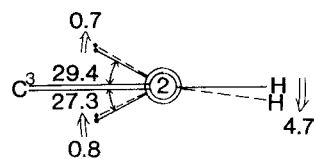
Wipff and Morokuma[11] and Spanget-Larsen and Gleiter[12a,b] argued that the CH bond is 'bent' owing to the repulsion between the methano bridge and the π electrons (Scheme 5). Schleyer[8] and Burkert[21] considered the bending to be due to the repulsion between

Scheme 5

the bridgehead hydrogens and the olefinic hydrogens, i.e. the torsional effect (Scheme 6).

Houk *et al.*[17b] considered the 'banana' orbitals produced by mixing the alkene σ and π orbitals, and proposed that both the torsional strain between the banana orbital and the methano bridge and that between the bridgehead hydrogen and olefinic hydrogen cause the 'rotation' of the alkenyl hydrogen (Scheme 7).

Scheme 6

Scheme 7

One question then is whether the π orbital is 'bent' or 'rotated.' The geometry of norbornene optimized under the constraint that the olefinic hydrogen atoms are coplanar with the C-1—C-2—C-3—C-4 plane is very similar to the fully optimized geometry in Figure 1, and gives no clear indication. Therefore, we considered the charge centroids of localized 'banana' bonds. If the 'bending' is taking place, the charge centroid should rotate around the C-2—C-3 axis. If the 'rotation' is taking place, it should rotate around the C-2—C-1 and C-4—C-3 axes. The localized 'banana' bonds were calculated with the Boys localization method[22] and the charge centroids were determined for the planar and the fully optimized norbornene. The locations of the centroids thus calculated are shown in Figure 9. Figure 9(A) shows that the charge centroids are rotated around
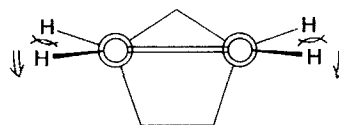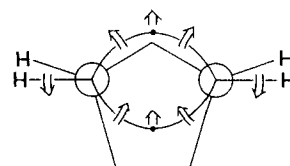

A. Bending

B. Rotation

Figure 9. Locations of charge centroids, marked with dots, for the fully optimized geometry (dashed lines) and the geometry optimized under the coplanar constraint (solid lines, Fig. 10). (A) 'Bending'; (B) 'rotation'
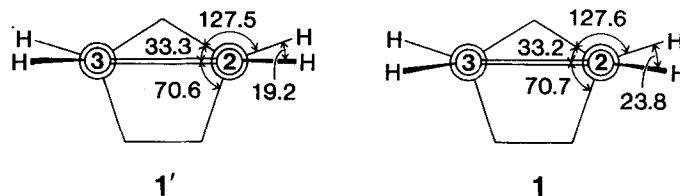
Scheme 8

the C-2—C-3 axis, by 1·7 (on the *exo* side)–1·9°(endo). Figure 9(B) also shows that the charge centroids are rotated around the C-2—C-1 and C-3—C-4 axes by 0·7(*exo*)–0·8°(*endo*), indicating that 'rotation' also takes place but to a smaller extent than 'bending.'

Energetic considerations

The energy difference between the fully optimized structure and the structure optimized under the C-1—C-2H—C-3H—C-4 coplanar restriction is 0·2 kcal mol^{-1}. In ethylene the structure optimized under the restriction (C_{2v}) that one HCCH plane is bent from the other by 4·8°, the bending angle in the fully optimized norbornene is found to be about 0·3 kcal mol^{-1} higher in energy than the fully optimized (D_{2h}) structure. Therefore, there has to exist roughly 0·2 + 0·3 = 0·5 kcal mol^{-1} of extra stabilization energy (pyramidalization energy) for norbornene.

In Scheme 8, we compare the dihedral angles around the C-2—C-1 and the C-3—C-4 axis of norbornene between the fully optimized geometry 1 and the optimized geometry 1' under the coplanar C-1—C-2H—C-3H—C-4 restriction. On releasing the coplanar restriction, the torsional angle between the bridgehead hydrogen and the olefinic hydrogen increases from 19·2° to 23·8°. The torsional energy contribution to the pyramidalization energy, i.e. the stabilization due to the change in this dihedral angle, is estimated, with the method in Scheme 3, to be about 0·2 kcal mol^{-1}. The effect of the small C-1—C-2—C-3 angle on the bending has been found to have a very small energetic contribu-

tion. We conclude here by saying that the norbornene pyramidalization energy is small and that no single factor emerges as its primary origin.

Most interesting, however, is that this small energy difference between the pyramidalized and the planar structures is amplified into a very large difference in the reactivity between norbornene *exo* and *endo* side.

COMPARISON BETWEEN NORBORNENE AND BICYCLO[2.1.1]HEX-2-ENE (9)

Here we concentrate on the difference in the reactivity between the *exo* side of norbornene and bicyclo[2.1.1]hex-2-ene (9), where both compounds have a cyclopentene skeleton on the reacting side of the olefinic double bond and therefore have a similar steric environment. Experimentally, *exo*-norbornene is about 1·4 times more reactive than 9 to the attack of 2,4,6-trimethylbenzonitrile oxide (28), and 6·3 times more reactive for the attack of C-*p*-nitrobenzoyl-*N*-phenylnitrone (29).
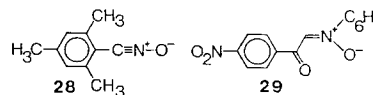
Discussions above have indicated that the *exo* – *endo* reactivity difference is due to the *endo* deformability. The symmetric bicyclo[2.1.1]hex-2-ene (9) is expected to have a planar olefinic group. Here we examine only the activation barrier E_a (transition state – reactant) and try to clarify the origin of the difference between *exo*-norbornene and bicyclohexene (9).
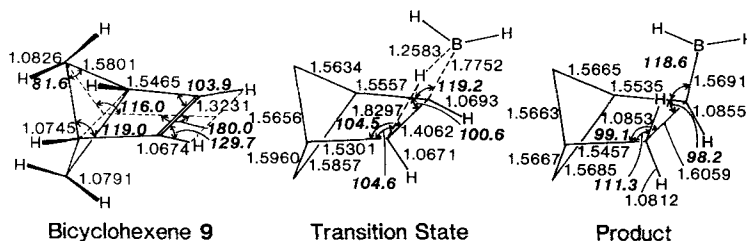

Bicyclohexene 9   Transition State   Product

Figure 10. HF/3–21G optimized geometries of 9, the transition state and the product of BH₃ addition. See text for restrictions on CH bond distances

Geometries and energetics

The geometries of the transition state and the reaction product for hydroboration of **9**, and also **9** itself, were optimized at the HF/3–21G level and are shown in Figure 10. We use the same assumption as in norbornene that non-olefinic CH bond distances at the transition state and the product (shown with bold lines for **9**) are those of optimized **9**. The optimized structure of **9** has C_{2v} symmetry, without pyramidalization of olefinic units. A comparison of geometrical parameters of the cyclopentene skeleton among norbornene, bicyclohexene (**9**) and cyclopentene is shown in Table 5. The angle between the plane of the methano bridge and the plane of the ethylene bridge, C-1—C-2—C-3 bond angle and the bond distances b and c all indicate that bicyclohexene (**9**) has more strain energy than norbornene, caused by the existence of the C-1—C-5—C-4—C-6 cyclobutane skeleton. The geometries of four atom reaction centres in Figures 4 and 10 indicate that the transition state for **9** is earlier than that for norbornene.

The energetics of the reaction of **9** are shown in Figure 3. The activation energy E_a for **9** is higher than that of norbornene by $1 \cdot 5 \, \mathrm{kcal \, mol^{-1}}$, but this difference is much smaller than the norbornene $exo - endo$ difference of $8 \cdot 8 \, \mathrm{kcal \, mol^{-1}}$. This is consistent with the experimental observation that the reac-

tivity of **9** and norbornene $endo$ side are about 10% and 0·5%, respectively, of that of norbornene exo side.[1,2] Interestingly, the exothermicity of BH_3 addition to **9**, $48 \, \mathrm{kcal \, mol^{-1}}$ at this level of calculation, is larger, by about $10 \, \mathrm{kcal \, mol^{-1}}$, than that of norbornene, despite the fact that the activation energy is smaller. The larger strain energy of **9** is released in the product as the result of the reaction that converted a double bond to a single bond. The larger exothermicity of **9** is consistent with the earlier transition state.

Deformation and interaction contributions to the barrier difference

Table 6 shows the results of the deformation and interaction energy analysis of the barrier height E_a. The trend for each contribution is similar to that in Δ(norbornene, $exo - endo$) in Table 2: $\Delta E_a < 0$, $\Delta DEF(\mathrm{olefin}) < 0$, $\Delta DEF(\mathrm{BH_3}) > 0$ and $\Delta INT < 0$. The major difference between $\Delta(exo - endo)$ and $\Delta(exo - 9)$ is that the magnitude of $\Delta DEF(\mathrm{olefin})$ is much smaller in the latter. Although it appears that $\Delta DEF(\mathrm{olefin})$ is still playing a major role, a further analysis of various effects, as was done above, is needed.
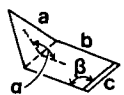
Model calculations for various origins

Endo *deformability*

The dihedral angles around the C-2—C-3 axis in the transition state of **9**, shown in Figure 5, suggest that the amount of bending required to reach the transition state and therefore the bending energy increase in the order norbornene exo side < bicyclohexene < norbornene $endo$ side, consistent with the deformation energy $DEF(\mathrm{olefin})$ in Tables 2 and 6.

The olefinic $endo$ deformability contribution to the deformation energy $DEF(\mathrm{olefin})$ in **9**, calculated using the method in Scheme 4, is $9 \cdot 1 \, \mathrm{kcal \, mol^{-1}}$ at the HF/3–21G level, compared with $7 \cdot 0 \, \mathrm{kcal \, mol^{-1}}$ for norbornene exo reaction mentioned above. Therefore, the

Table 5. Comparison of optimized geometrical parameters[a] of cyclopentene skeleton

	$\alpha \, (°)$	$\beta \, (°)$	$a \, (\text{Å})$	$b \, (\text{Å})$	$c \, (\text{Å})$
Bicyclohexene (**9**)	116·0	103·9	1·5801	1·5465	1·3231
Norbornene	127·9	107·9	1·5524	1·5303	1·3226
Cyclopentene	161·2	112·6	1·5623	1·5217	1·3174

[a] At the HF/3–21G level.

Table 6. Energy contributions to the reaction barrier E_a for bicyclo[2.1.1]hex-2-ene and norbornene

Method	Component	Norbornene *exo*	Bicyclohexene (**9**)	$\Delta(exo - 9)$
HF/3–21G	E_a	5·3	6·8	−1·5
	$DEF(\mathrm{olefin})$	14·2	16·3	−2·1
	$DEF(\mathrm{BH_3})$	22·6	21·2	1·4
	INT	−31·5	−30·7	−0·8
MP2/6–31G	E_a	−5·6	−3·7	−1·9
	$DEF(\mathrm{olefin})$	7·2	8·6	−1·4
	$DEF(\mathrm{BH_3})$	21·5	20·2	1·3
	INT	−34·3	−32·5	−1·8

[a] Energies in $\mathrm{kcal \, mol^{-1}}$ at the HF/3–21G optimized geometries. The total energy at the transition state of **9** is −256·7174 (HF/3–21G) and −258·6490 hartree (MP2/6–31G).

Table 7. Origins of activation energy difference ΔE_a (in kcal mol^{-1}) between norbornene *exo* side and bicyclo[2.1.1]hex-2-ene[a]

Method	*Endo* deformability	Staggering effect	Steric effect	ΔE
HF/3–21G	$-2 \cdot 1$	$-0 \cdot 6$	$+1 \cdot 2$	$-1 \cdot 5$
MP2/6–31G	$-1 \cdot 5$	$-0 \cdot 5$	$+0 \cdot 1$	$-1 \cdot 9$

[a] At the HF/3–21G optimized geometries.

endo deformability contribution to the difference in the barrier between norbornene *exo* side and **9** is $7 \cdot 0 - 9 \cdot 1 = -2 \cdot 1$ kcal mol^{-1}. Results at higher levels for the same geometries give $7 \cdot 1 - 9 \cdot 0 = -1 \cdot 9$ (HF/6–31G) and $4 \cdot 7 - 6 \cdot 2 = -1 \cdot 5$ kcal mol^{-1} (MP2/6–31G), as summarized in the second column of Table 7. On comparing Tables 6 and 7, it can be seen that the magnitude of the *endo* deformability contribution is equal to or slightly larger than the deformation energy *DEF*(olefin). This implies that the deformation energy of the skeleton part is smaller in bicyclohexene than in norbornene *exo* side. On the other hand, the changes in the dihedral angles around the C-1—C-4 axis on going from the reactant to the transition state in **9**, $3 \cdot 9°$ and $2 \cdot 5°$, as shown in Figure 6, are larger than the corresponding values in norbornene, $1 \cdot 4°$ and $2 \cdot 8°$, respectively. These observations can be explained by considering a large skeleton strain energy in bicyclohexene (**9**). As BH$_3$ approaches, the sp^3 character increases at the alkene carbon atoms, releasing the strain energy caused by an inside bond angle that is smaller than 120°. This release of the strain energy is larger in the more strained bicyclohexene than in norbornene, and is more than sufficient to upset the structural changes in the skeleton. This idea is consistent with the larger exothermicity of the bicyclohexene reaction than the norbornene reaction (Figure 3).

Staggering effect

The dihedral angles around the C-1—C-2 and C-4—C-3 axes in the transition state of **9** are shown in Figure 7. The C-3····H bond nearly bisects the angle between the methano bridge C—C bond and the bridgehead C—H bond. The C-2····B bond forms a small angle, $36 \cdot 4°$, between the methano bridge C—C bond, less favourable in the staggering effect than in norbornene *exo* transition state, $47 \cdot 0°$.

The staggering effect has been estimated by the method in Scheme 1. The destabilization due to the orbital overlap between the C-3····H bond and the methano bridge with the CCCH diehedral angle = $62 \cdot 0°$ should be zero. The destabilization due to the overlap between the C····B bond and the methano bridge is $0 \cdot 9$ kcal mol^{-1} (HF/3–21G). The corre-

sponding destabilization for norbornene *exo* reaction was $0 \cdot 3$ kcal mol^{-1}. Therefore, $0 \cdot 3 - 0 \cdot 9 = -0 \cdot 6$ kcal mol^{-1} is the contribution of the staggering effect to the activation energy difference, as shown in Table 7 together with those at higher levels of calculation.

Steric effect

As previously, the steric effect was estimated as (ΔDEF − *endo* deformability) + (ΔINT − staggering effect) and is given in the fourth column in Table 7. The steric effect favours bicyclohexene over *norbornene exo* side. This is because the deformation of the BH$_3$ is larger in norbornene, $\Delta DEF(\text{BH}_3) = +1 \cdot 3 - 1 \cdot 4$ kcal mol^{-1}, owing to the lateness of the transition state.

Origin of norbornene exo side − bicyclohexene reactivity difference

As is shown in Table 7, the *endo* deformability is the principal reason why norbornene *exo* side is more reactive than bicyclohexene. The difference in *endo* deformability between norbornene *exo* side and bicyclohexene is smaller than that between norbornene *exo* and *endo* side and so is the difference in the reactivity.

The conclusion of the comparison among norbornene *exo* side, bicyclo[2.1.1]hex-2-ene and norbornene *endo* side is that the decrease in the reactivity in this order is a reflection of the degree of pyramidalization in the isolated reactant. Norbornene *exo* side, already pyramidalized, is the most reactive. Unpyramidalized bicyclohexene requires pyramidalization to reach the transition state. Norbornene *endo* side, which is pre-pyramidalized in the wrong direction, requires the largest repyramidalization energy. This conclusion can probably be extended easily to the reactivity of tricyclooctene (**30**), which is comparable to that of bicyclohexene (**9**).[2] Very interesting is the reactivity of bicyclooctene (**31**), which is probably comparable to that of *endo*-norbornene.[1,2] The supposedly planar olefinic group would suggest an *endo* deformability contribution comparable to that of bicyclohexene. Therefore, there have to be some other factors, probably both the staggering effect and the steric effect, that make this compound less reactive. This should be a subject for further study.

30

31
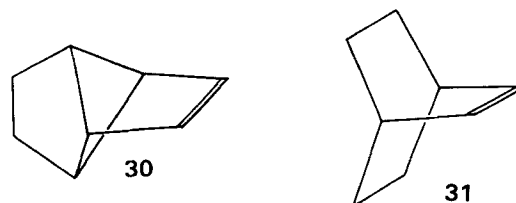
CONCLUSION

The geometries of the reactants, the reactant π-complex, the transition state and the product for *exo* and *endo* addition of BH_3 to norbornene were optimized at the HF/3–21G level, and their energies were calculated at up to the MP2/6–31G level. The activation energy analysis indicates that the energy required to deform the norbornene to reach the transition state for *exo* attack is smaller than that for *endo* attack and that this difference gives rise to the *exo* selectivity. In particular, *endo* deformability, a major portion of the norbornene deformation energy, is singled out as the origin of *exo* selectivity; norbornene, with the olefinic hydrogens already bent toward *endo* in the equilibrium geometry, requires less deformation to reach the *exo* than the *endo* transition state. A further analysis was carried out to elucidate the reason why olefinic hydrogens are bent in norbornene. A similar detailed analysis of the difference in the activation energy between norbornene *exo* side and bicyclo [2.1.1] hex-2-ene indicates that this difference is also dictated by the *endo* deformability.

REFERENCES

1. (a) H. C. Brown, *Chem. Br.* **2**, 199 (1966); (b) H. C. Brown, *J. Am. Chem. Soc.* **92**, 1990 (1970).
2. R. Huisgen, P. H. J. Ooms, M. Mingin and N. L. Allinger, *J. Am. Chem. Soc.* **102**, 3951 (1980).
3. (a) H. C. Brown, J. H. Kawakami and K. Liu, *J. Am. Chem. Soc.* **95**, 2209 (1973); (b) N. Takaishi, Y. Fujikura and Y. Inamoto, *J. Org. Chem.* **40**, 3767 (1975); (c) Y. Fujikura, Y. Inamoto, N. Takaishi, H. Ikeda and K. Aigami, *J. Chem. Soc., Perkin Trans. 1* 2133 (1976); (d) N. Takaishi, Y. Inamoto and K. Aigami, *Chem. Lett.* 803 (1979).
4. (a) H. C. Brown, J. H. Kawakami and S. Ikegami, *J. Am. Chem. Soc.* **92**, 6914 (1970); (b) L. A. Paquette, R. V. C. Carr, E. Arnold and J. Clardy, *J. Org. Chem.* **45**, 4907 (1980).
5. (a) L. A. Paquette, P. Charumilind, T. M. Kravetz, M. C. Böhm and R. Gleiter, *J. Am. Chem. Soc.* **105**, 3126 (1983); (b) L. A. Paquette, T. M. Kravetz, M. C. Böhm and R. Gleiter, *J. Org. Chem.* **48**, 1250 (1983).
6. (a) M. C. Böhm, R. V. C. Carr, R. Gleiter and L. A. Paquette, *J. Am. Chem. Soc.* **102**, 7218 (1980); (b) W. N. Washburm and R. A. Hillson, *J. Am. Chem. Soc.* **106**, 4575 (1984).
7. (a) T. Sugimoto, Y. Kobuke and J. Fukumoto, *J. Org.*
Chem. **41**, 1457 (1976); (b) P. H. Mazzochi, B. Stahly, J. Dodd, N. G. Rondan, L. N. Domelsmith, M. D. Rozeboom, P. Caramella and K. N. Houk, *J. Am. Chem. Soc.* **102**, 6482 (1980); (c) L. A. Paquette, R. V. C. Carr, P. Charumiling and J. F. Blount, *J. Org. Chem.* **45**, 4922 (1980); (d) M. Avenati, J. P. Hagenbuch, C. Mahaim and P. Vogel, *Tetrahedron Lett.* **21**, 3167 (1980); (e) P. D. Bartlett, A. A. M. Root and N. Shimizu, *J. Am. Chem. Soc.* **104**, 3130 (1982); (f) R. Subramanyam, P. D. Bartlett, G. Y. M. Iglesias, W. H. Watson and J. Galloy, *J. Org. Chem.* **47**, 4491 (1982); (g) L. A. Paquette, P. C. Hayes, P. Charumiling, M. C. Böhm, R. Gleiter and J. F. Blount, *J. Am. Chem. Soc.* **105**, 3148 (1983); (h) L. A. Paquette, A. G. Schaefer and J. F. Blount, *J. Am. Chem. Soc.* **105**, 3642 (1983); (i) P. D. Bartlett and C. Wu, *J. Org. Chem.* **49**, 1880 (1984).
8. P. v. R. Schleyer, *J. Am. Chem. Soc.* **89**, 701 (1967).
9. S. Inagaki, H. Fujimoto and K. Fukui, *J. Am. Chem. Soc.* **98**, 4054 (1976).
10. N. G. Rondan, M. N. Paddon-Row, P. Caramella, J. Marada, H. Muller and K. N. Houk, *J. Am. Chem. Soc.* **104**, 4974 (1982).
11. G. Wipff and K. Morokuma, *Tetrahedron Lett.* **21**, 4445 (1980).
12. (a) J. Spanget-Larsen and R. Gleiter, *Tetrahedron Lett.* **23**, 2435 (1982); (b) J. Spanget-Larsen and R. Gleiter, *Tetrahedron* **39**, 3345 (1983); (c) P. Carrupt and P. Vogel, *J. Mol. Struct.* **124**, 9 (1985).
13. J. S. Binkley, J. A. Pople and W. J. Hehre, *J. Am. Chem. Soc.* **102**, 939 (1980).
14. (a) J. A. Pople, J. S. Binkley and R. Seeger, *Int. J. Quantum Chem.* **S10**, 1 (1976); (b) R. Krishnan and J. A. Pople, *Int. J. Quantum Chem.* **14**, 91 (1978).
15. (a) W. J. Hehre, R. Ditchfield and J. A. Pople, *J. Chem. Phys.* **56**, 2257 (1972); (b) J. D. Dill and J. A. Pople, *J. Chem. Phys.* **62**, 2921 (1975).
16. J. S. Binkley, M. J. Frisch, D. J. DeFrees, K. Raghavachari, R. A. Whiteside, H. B. Schlegel and J. A. Pople, Gaussian 82, Carnegie–Mellon Chemistry Publishing Unit, Pittsburgh (1984).
17. (a) N. G. Rondan, M. N. Paddon-Row, P. Caramella and K. N. Houk, *J. Am. Chem. Soc.* **103**, 2436 (1981); (b) K. N. Houk, N. G. Rondan, F. K. Brown, W. L. Jorgensen, J. D. Madura and D. C. Spellmeyer, *J. Am. Chem. Soc.* **105**, 5980 (1983).
18. (a) T. Clark and P. v. R. Schleyer, *J. Organomet. Chem.* **156**, 191 (1978); (b) K. R. Sundberg, G. D. Graham and W. N. Lipscomb, *J. Am. Chem. Soc.* **101**, 2863 (1979); (c) Y. Osanai and H. Kashiwagi, *Int. J. Quantum Chem.* **17**, 1031 (1980); (d) S. Nagase, N. K. Ray and K. Morokuma, *J. Am. Chem. Soc.* **102**, 4536 (1980); (e) M. Sana and G. Leroy, *J. Mol. Struct.* **109**, 251 (1984); (f) K. N. Houk, N. G. Rondan, Y. D. Wu, J. T. Metz and M. N. Paddon-Row, *Tetrahedron* **40**, 2257 (1984); (g) T. Ozawa, N. Koga and K. Morokuma, unpublished results.
19. (a) T. Ozawa, N. Koga and K. Morokuma, unpublished results; (b) T. P. Fehlner, *J. Am. Chem. Soc.* **93**, 6366 (1971).
20. (a) K. Morokuma, *J. Chem. Phys.* **55**, 1236 (1971); (b) K. Morokuma and K. Kitaura, p. 215, in *Chemical Application of Atomic and Molecular Electrostatic Potentials*, edited by P. Politzer and D. G. Truhler. Plenum Press, New York (1981); (c) S. Nagase and K. Morokuma, *J. Am. Chem. Soc.* **100**, 1666 (1987).

21. U. Burkert, *Angew. Chem., Int. Ed. Engl.* **20**, 572 (1981).
22. S. F. Boys, in *Quantum Theory of Atoms, Molecules, and* *Solid States*, edited by P.-O. Löwdin, p. 629. Academic Press, New York (1966).